

Kinetic Phases in the Electron Transfer from $P^+Q_A^-Q_B$ to $P^+Q_AQ_B^-$ and the Associated Processes in *Rhodobacter sphaeroides* R-26 Reaction Centers[†]

Jiali Li,[‡] Dan Gilroy,[‡] David M. Tiede,[§] and M. R. Gunner*,[‡]

Department of Physics, Room J419, City College of New York, 138th Street and Convent Avenue, New York, New York 10031, and Chemistry Division D-200, Argonne National Laboratory, Argonne, Illinois 60439

Received July 14, 1997; Revised Manuscript Received December 23, 1997

ABSTRACT: Electron transfer from $P^+Q_A^-Q_B$ to form $P^+Q_AQ_B^-$ was measured in *Rhodobacter sphaeroides* R-26 reaction centers (RCs) where the native primary quinone, ubiquinone-10 (UQ_A), was replaced by 2-methyl-3-phytyl-1,4-naphthoquinone (MQ_A). The native secondary quinone, UQ-10, was retained as UQ_B. The difference spectrum of the semiquinone MQ_A⁻ minus UQ_B⁻ absorption is very similar to that of MQ⁻ minus UQ⁻ in solution (398–480 nm). Thus, the absorption change provides a direct monitor of the electron transfer from MQ_A⁻ to UQ_B. In contrast, when both Q_A and Q_B are UQ-10 the spectral difference between UQ_A⁻ and UQ_B⁻ arises from electrochromic responses of RC chromophores. Three kinetic processes are seen in the near UV (390–480 nm) and near-IR (740–820 nm). Analysis of the time-correlated spectra support the conclusion that the changes at $\tau_1 \approx 3 \mu\text{s}$ are mostly due to electron transfer, electron transfer and charge compensation are mixed in $\tau_2 \approx 80 \mu\text{s}$, while little or no electron transfer occurs at 200–600 μs (τ_3) in MQAUQ_B RCs. The 80- μs rate has been previously observed, while the fast component has not. The fast phase represents 60% of the electron-transfer reaction (398 nm). The activation energy for electron transfer is $\Delta G \approx 3.5 \text{ kcal/mol}$ for both τ_1 and τ_2 between 0 and 30 °C. In isolated RCs with UQ_A, if there is any fast component, it appears to be faster and less important than in the MQ_A reconstituted RCs.

Reaction centers (RCs) of purple non-sulfur photosynthetic bacteria store the energy of a photon by a series of electron-transfer reactions (1–3). Following absorption of a photon by a dimer of bacteriochlorophylls (P), the primary quinone (Q_A) is reduced in 200 ps forming $P^+Q_A^-$. Electron transfer from Q_A to the secondary quinone Q_B has been measured to occur within 200 μs yielding $P^+Q_B^-$. Substoichiometric proton uptake by the protein occurs at this step (4, 5). When there is an available electron donor to P⁺ such as cytochrome *c*, the absorption of a second photon yields a dihydroquinone at the Q_B site as Q_B⁻ accepts a second electron with the concomitant binding of two protons onto the quinone. It appears that proton transfer precedes the second reduction

of Q_B (6). The final product of two cycles of electron transfer in vivo are two oxidized cytochromes in the cell periplasm and reduced dihydroubiquinone in the cell membrane. Thus, RCs use the quinones in the Q_A and Q_B sites to create a two-electron gate where the single-electron donors and acceptors cytochrome *c*, P, and Q_A yield a doubly reduced, protonated product Q_BH₂ (7, 8).

The electron transfers from Q_A to Q_B have been the subject of much study (9, 10). This reaction starts the process of coupling electron and proton transfer in RCs and has been used as a model of this crucial step in the vectorial energy transfer and storage process (11, 12). RCs are one of the few energy-coupling, intrinsic membrane proteins where the atomic resolution structure is known. In addition, as this is a photosynthetic protein, single turnover reactions can be measured. The reaction has been studied by site-directed mutagenesis (10, 13), by a variety of spectroscopic techniques (14), and by theoretical analysis (15, 16). It is well-established that the first electron transfer does not involve proton binding by Q_B⁻ as indicated by optical (17), EPR (18), and ENDOR (19) measurements. The reaction does result in substoichiometric proton uptake from the surroundings and proton rearrangement within the protein (4, 5, 20–23). The electron transfer from Q_A to Q_B is the only intra-RC electron transfer that shows significant temperature and pH dependence (2, 24). In this, it is different from the other intra-RC reactions that proceed with less than a 5-fold change in rate from room temperature to 1 K. Thus, analysis of the quinone-dependent reactions must consider that protein or proton motions may control the electron-transfer rate.

* Author to whom correspondence should be addressed. Telephone: 212-650-5557. Fax: 212-650-6940. E-mail: gunner@scisun.sci.ccny.cuny.edu.

[†] City College of New York.

[‡] Argonne National Laboratory.

[§] Abbreviations: P, bacteriochlorophyll dimer which is the electron donor in the reaction center protein; BPh_M, bacteriopheophytin near Q_A on the L branch of the protein while BPh_M is near Q_B on the M branch; MQ, 2-methyl-3-phytyl-1,4-naphthoquinone; UQ, ubiquinone-10 (2,3-dimethoxy-5-methyl-6-decaisopropyl-1,4-benzoquinone); P⁺Q⁻ difference spectrum is the absorption of P⁺Q⁻ minus that of PQ; Q⁻ spectrum is the semiquinone minus quinone spectrum; k_{AB} is the rate constant of the electron transfer from P⁺Q_A⁻ to P⁺Q_B⁻ which includes all associated processes. Lifetimes for reactions: τ_{AP} for P⁺Q_A⁻ → PQ_A; τ_{BP} for P⁺Q_B⁻ → PQ_B; τ_{AB} for P⁺Q_A⁻Q_B → P⁺Q_AQ_B⁻. τ_{AB} was analyzed as the sum of three exponentials with lifetimes τ_1 , τ_2 , and τ_3 and respective amplitudes A₁, A₂, and A₃.

The basic problem with studying the electron transfer from Q_A to Q_B in RCs from *Rhodobacter sphaeroides* is that the same quinone, ubiquinone-10, is found in both quinone binding sites. In the near-UV region of the spectra, the light-induced absorbance changes are almost identical for the reduction of UQ_A or UQ_B and are similar to that obtained for ubisemiquinone in alcoholic solution (17, 25). Therefore, there is no primary optical marker to distinguish between the semiquinone states UQ_A^- and UQ_B^- . Instead, secondary signals have been used including (1) changes in the spectrum of the bacteriopheophytins adjacent to the quinones at 750 or 770 nm (17, 26), (2) small differences in the absorbance of UQ_A^- and UQ_B^- at 397 nm (7, 17, 27, 28), (3) changes in the protein and quinone vibrations monitored at 1430–1780 cm^{-1} (20, 21), and (4) the recovery of P's competence to initiate a second turnover of electron transfer, a process which cannot occur until Q_A^- has been oxidized by Q_B (29, 30). All measurements show a process with a lifetime between 100 and 300 μs ($3300\text{--}10\,000\text{ s}^{-1}$) at room temperature and pH 7–8 in native RCs of *Rb. sphaeroides* that has been assigned to the first electron transfer from Q_A^- to Q_B (7, 17, 30). Recent measurements have shown that the reaction has other phases, with both faster (26) and slower (27) components. Unfortunately, the secondary, electrochromic markers which monitor the charge distribution cannot easily distinguish between electron transfer or secondary processes such as proton transfer or protein rearrangement. However, the direct optical observation of electron transfer from Q_A^- to Q_B in *Rb. sphaeroides* RCs can be made if the ubiquinone-10 (UQ_{10}) in the Q_A site is substituted by 2-methyl-3-phytyl-1,4-naphthoquinone (MQ_A), while UQ_{10} is retained as Q_B . The spectrum of menasemiquinone (MQ^- , λ_{max} at 400 nm) is different from ubisemiquinone (UQ^- , λ_{max} at 450 nm) (31–33), providing a direct monitor of the electron transfer from MQ_A^- to UQ_B .

The replacement of UQ_A by MQ_A is expected to modify the Q_A^- to Q_B electron transfer very little. Although MQ is 140 meV harder to reduce in aqueous solution than UQ, in the *Rb. sphaeroides* Q_A site MQ_A and UQ_A have reduction potentials that differ by only 30 meV (34). In addition, crystallographic structures (35) and FTIR measurements (36) show that MQ_A and UQ_A have very similar interactions with the protein. The use of MQ_A and UQ_B mimics the native quinone complement in *Rhodopseudomonas viridis* RCs (33). Specific quinone substitution succeeds because the Q_A site in *Rhodobacter sphaeroides* RCs has a preference for MQ over UQ (37). In addition, menaquinone will not function as Q_B when Q_A is UQ or MQ, so only electron transfer from MQ_A^- to UQ_B occurs (38).

MATERIALS AND METHODS

Protein Isolation. *Rb. sphaeroides* R-26 reaction centers were isolated following standard procedures using lauryldimethylamine-N-oxide (LDAO, Calbiochem) detergent extraction followed by purification using ammonium sulfate and DEAE chromatography (39). Q_A and Q_B were removed with orthophenanthroline using the method of Okamura (40), with minor modifications (34). This typically yields RCs with no Q_B and $\approx 5\% Q_A$. The RC concentration was measured at 802 or 865 nm given the following extinction coefficients: $\epsilon_{802} = 0.288 \mu\text{M}^{-1} \text{cm}^{-1}$ or $\epsilon_{865} = 0.135 \mu\text{M}^{-1} \text{cm}^{-1}$.

Quinone Reconstitution. The long-tailed quinones are effectively insoluble in water, but become soluble when detergent is added. However, detergent weakens the affinity of quinone for the binding sites. The method of Wraight (41) using quinone dissolved in Triton X-100 was the basis of the most effective and reproducible method of reconstitution. Quinone solutions of 1 mM MQ (2-methyl-3-phytyl-1,4-naphthoquinone, Vitamin K1, Fluka) or 10 mM UQ_{10} (Sigma or Fluka) were heated for 5–10 s in a microwave oven to dissolve the quinone. The MQ used here is a close analogue to MQ_4 or UQ_4 ; however, the tail has one isoprenyl unit and three isopranyl (saturated isoprenyl) units on the end of the tail. A final concentration of 1.2–1.6 MQ/RC was added to a 4–5 μM RC solution with 0.02% Triton X-100 at room temperature. Complete MQ_A reconstitution was verified by comparing RC light-initiated electron transfer at 430 nm before and after addition of 2-methyl-1,4-naphthoquinone (MQ_0). The water soluble MQ_0 rapidly fills any empty Q_A sites, increasing the activity. Samples were also checked for recovery of the ground state from the $P^+Q_A^-$ state with $\tau_{AP} \approx 75 \text{ ms}$, characteristic of electron transfer from MQ_A^- to P^+ . If UQ is Q_A , τ_{AP} is 100 ms. Following complete reconstitution of the Q_A site, the Q_B site was reconstituted with UQ_{10} at $\approx 15 \text{ UQ/RC}$. The final UQ_B occupancy was above 95%.

Due to the competition between MQ and UQ_{10} for the Q_A site, a small fraction of the Q_A sites were occupied by a UQ_{10} . The fraction of MQ as Q_A was determined from the charge recombination kinetics given the different k_{BP} 's in $P^+UQ_AUQ_B^-$ and in $P^+MQ_AUQ_B^-$ RCs. Approximately 85% of the Q_A binding sites contain MQ with 15% UQ_{10} occupancy. The different k_{BP} rate constants were fixed during the two-exponential fitting.

Charge recombination kinetics were measured at 430 nm, pH 8.0, room temperature ($22 \pm 2^\circ\text{C}$), 10 mM Tris, and 4–5 μM RC, with 0.02–0.03% Triton X-100 for four types of RCs. Without Q_B , τ_{AP} is 75 ms ($k_{AP} = 13.3 \pm 0.6/\text{s}$) from $P^+MQ_A^-$; 108 ms ($9.3 \pm 0.2/\text{s}$) from $P^+UQ_A^-$ (1.5 stigmatellin/RC added to remove any UQ_B (Fluka)). When Q_B is present, charge recombination at τ_{BP} is 2.8 s ($k_{BP} = 0.36 \pm 0.4/\text{s}$) from $P^+MQ_AUQ_B^-$; 1.19 s ($0.84 \pm 0.01/\text{s}$) from $P^+UQ_AUQ_B^-$. The driving force (ΔG) for electron transfer from Q_A^- to Q_B can be calculated from the charge recombination rates k_{AP} and k_{BP} (30, 42). The pathway for charge recombination in $P^+Q_B^-$ RCs is via Q_A^- (at k_{AP}) so that $P^+Q_A^-Q_B$ and $P^+Q_AQ_B^-$ come to equilibrium (K_{AB}) and then return to the ground state at

$$k_{BP} = k_{AP}/(K_{AB} + 1) \quad (1)$$

In UQ_AUQ_B RCs, the reaction ΔG is 60 meV; in MQ_AUQ_B RCs, it is 93 meV.

Optical Measurements. Light-induced absorbance changes were measured using a flash spectrophotometer designed by the University of Pennsylvania Biomedical Instrumentation Group. Actinic light was provided by a 5-ns, 532-nm pulsed YAG laser pumping the fluorescent dye LDS 751 (Exciton). The peak of the fluorescence was at 750 nm. The laser intensity was adjusted to provide 80–90% saturation of the P^+ signal. The measuring light, placed perpendicular to the excitation light, was from a 100-W quartz halogen–tungsten lamp (ORIEL) with appropriate neutral density and interfer-

ence filters and was controlled by a shutter placed before the RC sample which was only opened during measurement. For kinetic measurement of Q_A to Q_B , the shutter was opened for less than 10 ms. The transmitted light was detected using a Thorn EMI 9798QB photomultiplier. The output from the photomultiplier was amplified by a Stanford Research System model SR445 or Comlinear Model E103 fast amplifiers. For measurement of the $P^+Q_A^-Q_B$ to $P^+Q_AQ_B^-$ electron transfer, the amplified signal was sent to 2 LeCroy (model 9310M 300 MHz and 9304A 250 MHz) digital storage oscilloscopes, recording and averaging different time scales. The time resolution of the measuring system was limited by the 80 ns rise time of the photomultiplier tube. The time between flashes was 1–4 min and 50–60 kinetic traces were averaged.

Semiquinone spectra were measured 25 ms after a single saturating flash, in the presence of 200 ferrocene/RC. Ferrocene (Aldrich) was diluted in alcohol. With ferrocene as an electron donor to the bacteriochlorophyll dimer, charge recombination from $P^+Q_A^-$ or $P^+Q_AQ_B^-$ was prevented. Instead, a stable PQ_A^- or $PQ_AQ_B^-$ state is created which decays slowly, allowing clear observation of the semiquinone signal (43, 44). The time between flashes was 10 min. About 3–5 kinetic traces were averaged.

The measurements of time-resolved electrochromism associated with the formation of quinone anions at 760 nm were performed as described by Tiede et al. (26).

Data Analysis. The Levenberg–Marquardt algorithm, a nonlinear least-squares fitting in IGOR Pro (WaveMetrics) was used to analyze the kinetic traces by fitting to two or three exponentials plus a constant using the standard expression:

$$A(t) = A_0 + A_1 * \exp(-t/\tau_1) + A_2 * \exp(-t/\tau_2) + A_3 * \exp(-t/\tau_3) \quad (2)$$

Two sets of data were recorded simultaneously by the two digitizing oscilloscopes. In the time range 0–20 μ s, 2000 data points were collected. This kinetic trace was fit to a single exponential. In the time range 0–2 ms, 20 000 data points were collected. These data were averaged nonlinearly so that each kinetic component has similar data density to provide a total of 2700 data points. Thus, more data points were retained at early times. The fitting of the longer time scale data depended on the results of fitting the fast trace. If a fast component was seen in the 20- μ s data, the longer data set was fit with three exponentials. The fastest rate was fixed from the early time data. If there was no fast phase, the longer data set was fit to two exponentials. The following fitting methods were used for the different spectral components.

1. $P^+MQ_A^-$ or $P^+UQ_A^-$ show no changes at 398 nm for at least 1 ms. At times greater than 1.5 ms, the charge recombination of P^+Q^- begins to be observed. Analysis of the changes that depend on the presence of Q_B at this wavelength is carried out on the raw data.

2. At wavelengths other than 398 nm, the kinetic signal associated with Q_A^- to Q_B electron transfer is very small compared to the difference between the P^+ and P signal. In addition, the large ΔA from the flash-induced oxidation of P produces a small reproducible hysteresis in the PMT tube ($\tau \approx 200 \mu$ s). Therefore, analysis of the kinetic processes

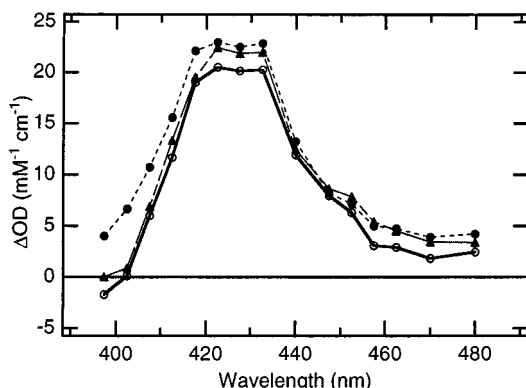


FIGURE 1: Light minus dark absorbance spectra of RCs without Q_B where Q_A is UQ_{10} (▲) or MQ_3 (●), RCs with MQ_AUQ_B (○). Change in optical density (ΔOD) measured 10 μ s after the flash, with 4 μ M RCs in 0.02% Triton, 10 mM Tris, 2.5 mM KCl at 22 °C, pH 8.0. The RC concentration was determined from the static extinction coefficients at 802 and 865 nm: $\epsilon_{802} = 0.288 \mu\text{M}^{-1} \text{cm}^{-1}$ or $\epsilon_{865} = 0.135 \mu\text{M}^{-1} \text{cm}^{-1}$.

associated with Q_B^- requires subtraction of $P^+Q_A^-$ kinetic traces from those obtained with a matched $P^+Q_AQ_B^-$ sample. The samples, with Q_A alone and both Q_A and Q_B present were reconstituted with Q_A in the same tube and then split. UQ_B was added to one sample. The concentration difference between the two samples is less than 1%.

RESULTS

The Spectrum of $P^+Q_A^-$, Q_A^- , and Q_B^- in the Near UV. From 398 to 480 nm the change in absorbance going from the ground state (PQ_AQ_B) to the $P^+Q_A^-$ state (denoted the $P^+Q_A^-$ spectrum) or to the $P^+Q_B^-$ state (the $P^+Q_B^-$ spectrum) is dominated by the changes in absorbance of P as it is oxidized. Replacing the native ubiquinone by menaquinone has little effect on the $P^+Q_A^-$ spectrum (Figure 1). The small increase in absorbance below 435 nm in the $P^+MQ_A^-$ spectrum arises because MQ^- absorbs more than UQ^- in this region (Figure 3a). The contribution of Q_A^- or Q_B^- to the spectra can only be seen clearly by the addition of an electron donor to P^+ , such as ferrocene. The semiquinone minus quinone difference spectra of UQ_A^- , $UQ_AUQ_B^-$ (Figure 2a), and $MQAUQ_B^-$ (Figure 2c) are very similar. Each of these intra-RC UQ species bears a strong resemblance to the UQ^- spectrum in solution (Figure 3a) (31).

The peak of the UQ^- spectrum at 445 nm in solution (Figure 3a) is red-shifted by 5 nm when it is UQ_A^- and by only 2 nm as UQ_B^- (Figure 2a). The main features of the UQ_B^- spectrum is independent of which quinone is in the Q_A site (Figure 2a,c). Thus, the peaks at 420, 445, and 460 nm in the $(UQ_A^-)-(UQ_AUQ_B^-)$ difference spectrum (Figure 2b) can be obtained simply by subtracting a solution spectrum shifted by 5 nm from one shifted by only 2 nm and multiplied by ≈ 1.2 . The only significant difference between the solution spectrum and the intra-RC UQ_A^- and UQ_B^- spectra is the peak in the UQ_A^- spectrum at 398 nm, which is not found in the UQ_B^- spectra. The amplitude of the absorbance difference between UQ_A^- and UQ_B^- (Figure 2b) is small compared to the changes associated with the oxidation of P (see Figure 1). The UQ_A^- peak at the P^+ minus P isobestic point near 400 nm provides the best window to follow Q_A to Q_B electron-transfer coupled processes. Unfortunately, this peak represents a still unassigned electrochromic shift

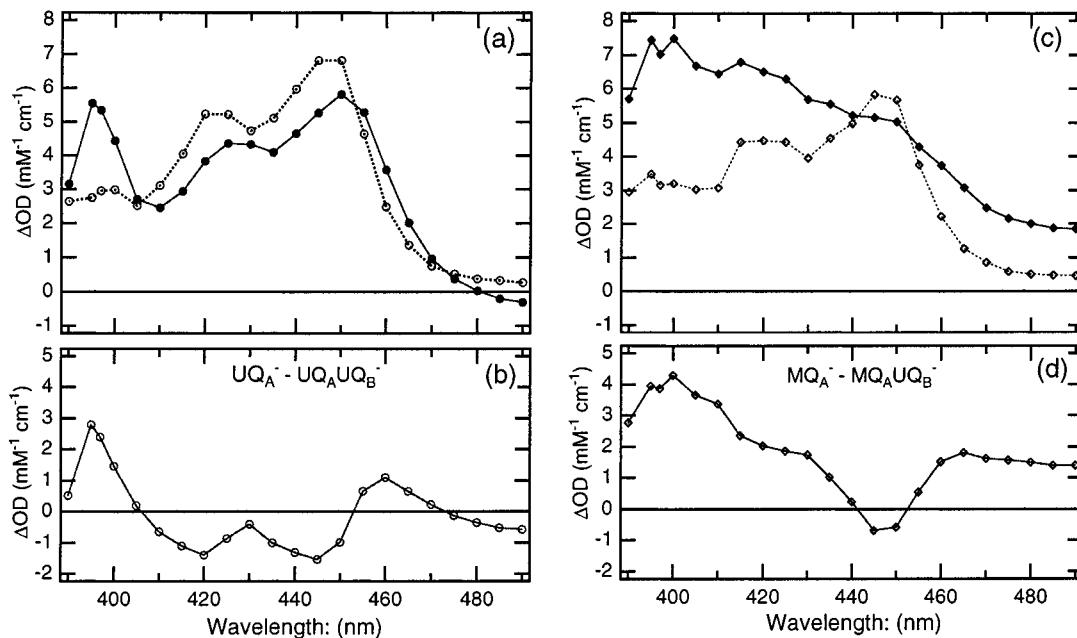


FIGURE 2: Light minus dark difference spectrum of 1 μM RCs with 200 μM ferrocene measured 25 ms after excitation flash. This provides the (semiquinone)–(quinone) spectra for (a) PUQA $^-$ (●), PUQAUQB $^-$ (○); (c) PMQA $^-$ (◆), PMQAUQB $^-$ (◇). Double difference spectrum of (b) PUQA $^-$ minus PUQAUQB $^-$; (d) PMQA $^-$ minus PMQAUQB $^-$. The Q $_B$ occupancy was normalized to 100%. About 3–5 measurements were averaged. Buffer conditions are the same as in Figure 1.

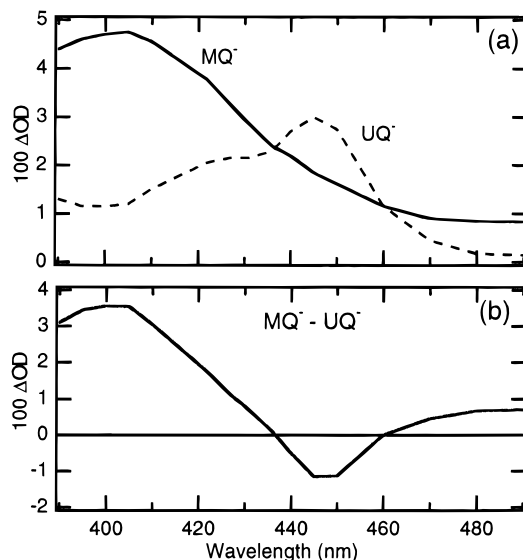


FIGURE 3: Semiquinone–quinone difference spectra in solution measured by pulse radiolysis in aqueous solution. (a) 100 μM MQ $^-$ (solid line) 5 M isopropyl alcohol pH = 6.4; 100 μM UQ $^-$ (dotted line) 7 M isopropyl alcohol, pH = 8. (b) Double-difference spectrum of MQ $^-$ minus UQ $^-$. Data taken from Patel and Willson (31).

of the quinone or other protein cofactor. It will be seen that this wavelength monitors later events as well as the electron-transfer itself.

While in the native *Rb. sphaeroides* RCs, Q $_A$ and Q $_B$ are the same compound, so there is no primary difference in their spectra. However, there is a significant difference in the semiquinone spectra of UQ and MQ. The maximum MQ $^-$ absorbance is at 400 nm in RCs and in solution, while the maximum for UQ in solution, or in the Q $_A$ or Q $_B$ sites, is near 450 nm. The absorbance difference of (MQ $_A^-$) minus (MQ $_A$ UQB $^-$) in MQ $_A$ reconstituted RCs (Figure 2d) looks very much like the difference between MQ $^-$ and UQ $^-$ in aqueous solution (Figure 3b) with the same peaks and

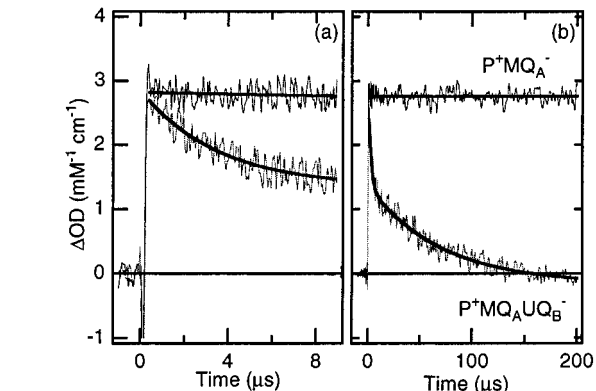


FIGURE 4: The kinetics of light-induced absorbance changes at 398 nm, pH = 8. (a) First 10 μs : RCs reconstituted with MQ $_A$ only (top), with both MQ $_A$ and UQB (bottom). τ_1 of 3.5 μs was obtained by single-exponential fitting to the bottom trace. (b) The same transient monitored for 200 μs . τ_2 is 87 μs obtained when τ_1 is fixed at 3.5 μs . Measurement conditions as in Figure 1.

troughs. There are additional features near 400, 420, and 465 nm. These peaks are found in the UQA $^-$ –UQB $^-$ spectrum. However, \approx 15% of the RCs with UQA does not fully account for the magnitude of the changes indicating small shifts of the MQ $^-$ spectrum as it binds to the protein, or changes in the protein spectrum in response to the formation of Q $_A^-$.

Absorption Changes Associated with Q $_A^-Q_B$ to Q $_AQ_B^-$ Electron Transfer. When RCs were reconstituted with MQ at the Q $_A$ site and UQ at the Q $_B$ site, at 398 nm three kinetic components were observed following the formation of P $^+$ MQ $_A^-$ UQB (Figure 4, summarized in Figure 9a). A fast absorbance change, $\tau_1 = 3.5 \pm 0.9 \mu\text{s}$ ($3.3 \times 10^5 \text{ s}^{-1}$) with $A_1 \approx 45\%$, an intermediate phase, $\tau_2 = 80 \pm 15 \mu\text{s}$ (12 500/s) with $A_2 \approx 25\%$, and a slow phase, $\tau_3 = 260 \pm 50 \mu\text{s}$ (3800/s) with $A_3 \approx 30\%$. These transients depend on the presence of UQB. With MQ at the Q $_A$ site and no Q $_B$, there is no change in the optical absorption for 1 ms. In P $^+$ MQ $_A^-$

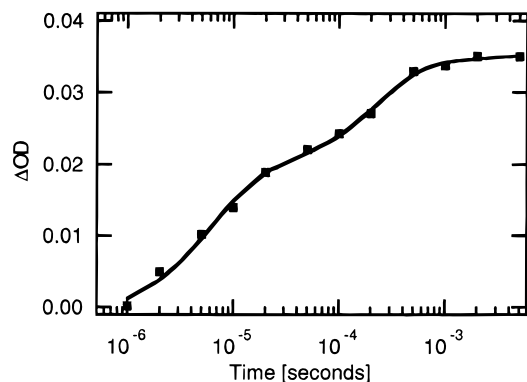


FIGURE 5: Absorbance changes in $\text{MQ}_\text{A}\text{UQ}_\text{B}$ RCs at 757 nm and 6 °C. Amplitude normalized to ΔOD (865 nm, 0 μs) = 1. Solid line fit to three exponentials: $\tau_1 = 6.3 \pm 1.2 \mu\text{s}$, $\tau_2 = 205 \pm 55 \mu\text{s}$, and $\tau_3 = 950 \pm 180 \mu\text{s}$ with relative amplitudes of 0.53, 0.39, and 0.08.

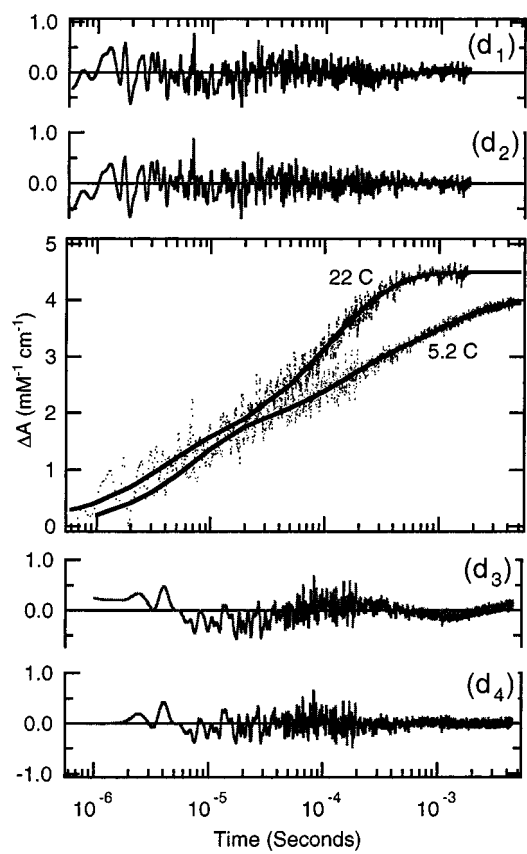


FIGURE 6: Kinetics of absorption change at 398 nm at 22 and 5.2 °C. Residuals of fitting 22 °C data with (d₁) two exponentials (3.5 and 130 μs) or (d₂) three exponentials (3.5, 78, and 260 μs) and 5.2 °C data with (d₃) two exponentials (7 and 490 μs) or (d₄) three exponentials (7, 120 and 1100 μs). 3 exponential fitting on data.

RCs, only charge recombination to the ground state at $\tau_{\text{AP}} = 75 \text{ ms}$ is seen. Stigmatellin, a competitive inhibitor of Q_B , removes all sub-millisecond components in $\text{MQ}_\text{A}\text{UQ}_\text{B}$ RCs. Thus, these three components are associated with electron transfer from MQ_A^- to UQ_B .

The two slower rates, $\tau_2 \approx 80 \mu\text{s}$ and $\tau_3 \approx 260 \mu\text{s}$, have been previously reported in $\text{UQ}_\text{A}\text{UQ}_\text{B}$ RCs (26, 27) (Figure 9). τ_1 is faster than previously reported in isolated RCs. However, as seen in Figure 4 the fast phase is a significant fraction of the processes that occur on electron transfer from Q_A^- to Q_B . The fast phase is clearly part of this reaction

since the initial absorbance amplitude for $\text{P}^+\text{Q}_\text{A}^-$ to $\text{P}^+\text{Q}_\text{B}^-$ electron-transfer kinetics must equal the absorbance of the starting state which is $\text{P}^+\text{Q}_\text{A}^-$. Having the same initial amplitude in a closely matched pair of samples with and without Q_B is the best way to check that none of the Q_A^- to Q_B reaction occurs faster than the time resolution of the measurements. When only the slower components are analyzed, $\approx 50\%$ of the absorbance change at 398 nm occurs as a burst phase (Figure 4b). A predicted absorbance change on reaction can also be derived from the difference in the absorbance of ferrocene-trapped MQ_A^- and UQ_B^- (Figure 2) which is $4.0 \pm 0.4 \Delta\text{OD}/\text{mM}$ at 400 nm (normalized to 100% Q_B reconstituted). The sum of the initial amplitudes of the τ_2 and τ_3 components is only 60% of the predicted value. Adding the τ_1 contribution, the value is within 90% of that expected.

The transient absorbance difference in $\text{MQ}_\text{A}\text{UQ}_\text{B}$ RCs was also measured at 757 nm at 6 °C (Figure 5). Three phases are seen: $\tau_1 = 6.3 \pm 1.2 \mu\text{s}$, $\tau_2 = 205 \pm 55 \mu\text{s}$ and $\tau_3 = 950 \pm 180 \mu\text{s}$ with relative amplitudes of 0.53, 0.39 and 0.08, respectively. These rates are similar to the rates observed at 398 nm at 5.2 °C where $\tau_1 = 6.6 \pm 0.5 \mu\text{s}$, $\tau_2 = 120 \pm 12 \mu\text{s}$ and $\tau_3 = 1.1 \pm 0.1 \text{ ms}$ with relative amplitudes of 0.41, 0.27, and 0.32, respectively (see Figures 6 and 9b).

The time course of the absorbance changes associated with the UQ_A^- to UQ_B electron-transfer reaction were also measured at 398 nm. At this wavelength, the two slower rates $\tau_2 = 65 \pm 25 \mu\text{s}$ and $\tau_3 = 260 \pm 50 \mu\text{s}$ seen in $\text{MQ}_\text{A}\text{UQ}_\text{B}$ RCs are clearly observed. A fast absorption change at $< 1 \mu\text{s}$, representing approximately 15% of the total amplitude, may also be seen. Unfortunately, this fast rate is at the limit of the instrument response time. No absorption changes are seen at 398 nm from 2 to 40 μs following the formation of $\text{P}^+\text{Q}_\text{A}^-$ in $\text{UQ}_\text{A}\text{UQ}_\text{B}$ RCs. The same results are found in RCs where both Q_A and Q_B are reconstituted with UQ_{10} as well as in RCs when UQ_A is retained during the purification procedure. Thus, the quinone extraction and replacement is not the cause of the difference between the MQ_A and UQ_A RCs.

Two- or Three-Exponential Curve Fitting. The rate constants obtained by fitting kinetic transients depend to some degree on the analysis method. The fast component τ_1 is 23 times faster than τ_2 , so it is clearly seen in $\text{MQ}_\text{A}\text{UQ}_\text{B}$ RCs. In contrast, the two slower components differ by only 3-fold so are harder to resolve. Fitting a kinetic trace obtained at room temperature, 398 nm, and pH 8 (Figure 6), to three exponentials yields τ 's of 3.5, 78, and 260 μs . Fitting the same data with two exponentials, gives τ 's of 3.5 and 130 μs . The improvement with the third component is small (see residuals in Figure 6). However, at lower temperature (5.2 °C) (Figure 6, bottom), τ_2 and τ_3 are better separated. Here, a two-exponential fit shows substantially more error than when three exponentials are used. The results at both low temperature and high pH (data not shown) where the second (τ_2) and third (τ_3) components are better separated demonstrate that there are at least three phases of absorbance changes. In addition, as will be seen below, τ_2 and τ_3 have different spectra. Therefore, all kinetic traces with Q_B were fitted to three exponentials.

Spectra of the Three Kinetic Components. The wavelength dependence of each kinetic component (the transient absorp-

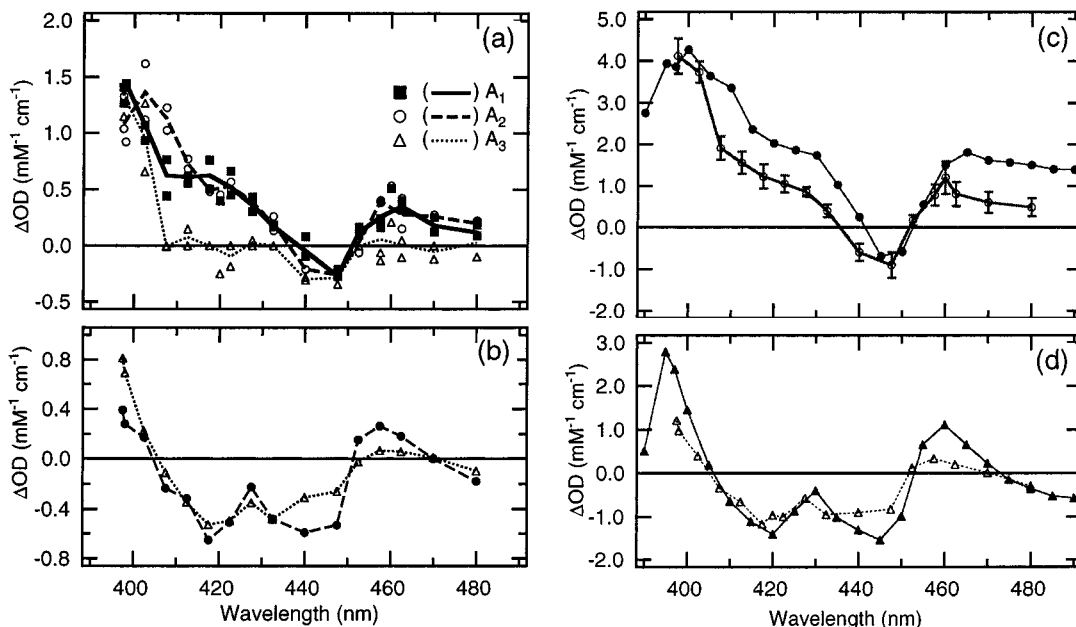


FIGURE 7: The spectra of each kinetic component. (a) MQ_AUQ_B RCs: A_1 (■), A_2 (○), A_3 (△). (b) UQ_AUQ_B RCs: A_2 (●), A_3 (△). (c) MQ_AUQ_B RCs: $A_1 + A_2 + A_3$ (○); double-difference spectrum measured with ferrocene as an electron donor from Figure 4b (●). (d) UQ_AUQ_B RCs: $A_2 + A_3$ (△) double-difference spectrum from Figure 2b (▲). Results in c and d normalized to 100% UQ_B .

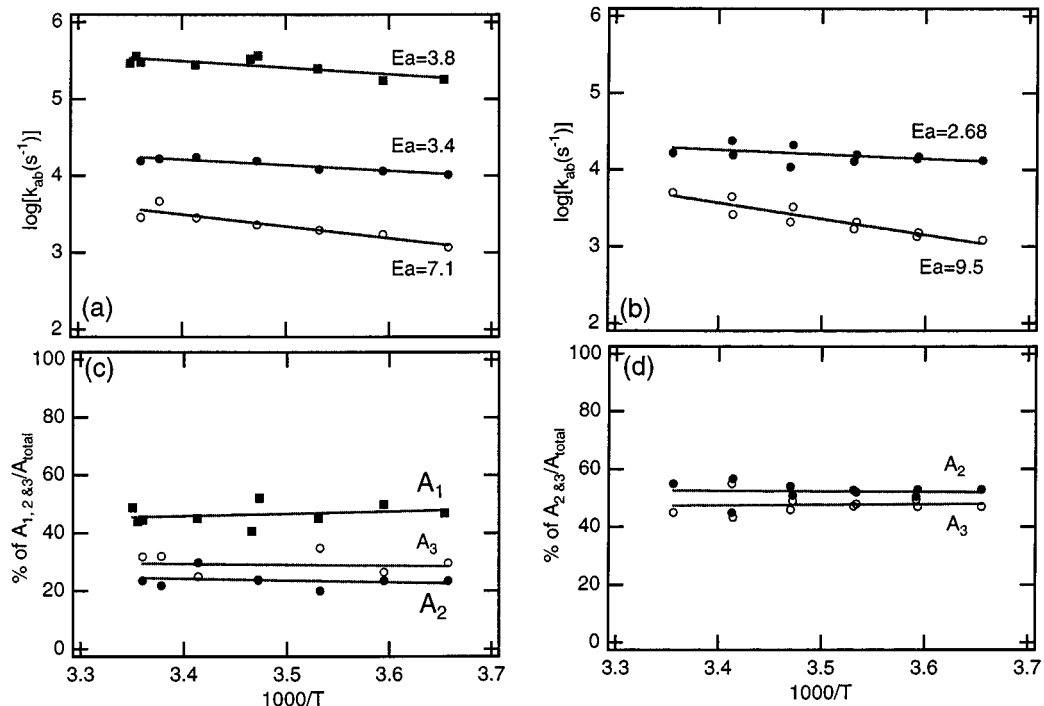


FIGURE 8: Temperature dependence of each kinetic component. The activation energies (E_a) are in kcal/mol. MQ_AUQ_B RCs: (a) Arrhenius plot for $k_1 = 1/\tau_1$ (■), $k_2 = 1/\tau_2$ (●) and $k_3 = 1/\tau_3$ (○). (c) Percentage of the total $\Delta A (=A_1 + A_2 + A_3)$ at A_1 (■), A_2 (●), and A_3 (○). UQ_AUQ_B RCs: (b) Arrhenius plot for $k_2 = 1/\tau_2$ (●) and $k_3 = 1/\tau_3$ (○). (d) Percentage of the total $\Delta A (=A_2 + A_3)$ at A_2 (●) and A_3 (○). The conditions were the same as in Figure 3 and all data were measured at 398 nm.

tion difference spectrum) can provide the information to identify the reaction occurring at this rate. In MQ_AUQ_B RCs, the shape of the transient absorption spectra with lifetimes of 3 and 80 μs (Figure 7a) largely matches the shape of the MQ^- minus UQ^- spectra in solution (Figure 3b). Thus, 60% of the electron transfer from MQ_A^- to UQ_B occurs with a lifetime of 3 μs while the remaining 40% of the MQ_A^- transfers its electron to UQ_B in 80 μs . In contrast, τ_3 (200–600 μs) is only measurable near 400 or 450 nm. Thus, the slow rate monitors other changes in the protein occurring

after electron transfer. This slow phase accounts for 30% of the total change at 398 nm in MQ_AUQ_B RCs.

The sum of the three components are in reasonable agreement with the difference spectrum predicted from ferrocene-trapped MQ_A^- minus UQ_B^- (Figure 7c), especially around 400 and 450 nm. At other wavelengths, while the shape of the spectrum matches qualitatively, there are differences between the amplitudes of the two curves (Figure 7c). The reason for the mismatch is unknown. One explanation for the static difference of MQ_A^- minus UQ_B^-

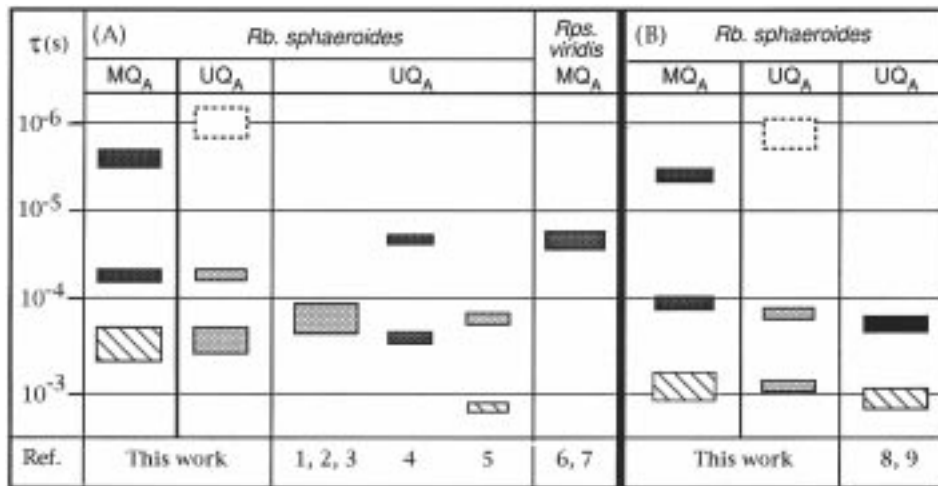


FIGURE 9: Summary of measured time constants of electron transfer from Q_A^- to Q_B and associated processes: (A) at room temperature; (B) at 4–6 °C. Black boxes are assigned to electron transfer and hatched boxes are assigned to proton uptake or protein rearrangement. The possibility of a fast τ_1 in UQ_A RCs is shown by the dashed border. The gray boxes are from measurements where the process monitored by a kinetic transient has not been assigned. Single-exponential fit to data at 750 nm: 1. Verméglia and Clayton (17); 2. Wraight (7); 3. Kleinfeld et al. (30). Double exponential fit of data at 757 nm: 4. Tiede et al. (26). At 397 nm: 5. Takahashi et al. (27). Double-flash method: 6. Leibl et al. (48); 7. Mathis et al. (82). FTIR measurements at 1725 cm^{-1} : 8. Hienerwadel et al. (20); 9. Hienerwadel et al. (21).

Table 1: Summary of Activation Energies (E_a)

RC\time constant at 22 °C	$\tau_1 = 3.5 \mu\text{s}$	$\tau_2 = 80 \mu\text{s}$	$\tau_3 = 200\text{--}600 \mu\text{s}$
$MQ_A UQ_B$ (kcal/mol)	3.8 ± 1.1	3.4 ± 0.6	7.1 ± 1.3
$UQ_A UQ_B$ (kcal/mol)	2.7 ± 1.2	9.5 ± 1.4	

being bigger than the amplitude change obtained from the kinetic results (Figure 7c) is that the trapped semiquinone spectrum was measured 25 ms after the flash rather than being limited to the 2 ms observed in the kinetic measurements. Thus, the static states of MQ_A^- and UQ_B^- in RCs where charge recombination is blocked may include additional proton uptake or protein conformational changes that add to the difference spectra.

In $UQ_A UQ_B$ RCs, the only evidence for the fast component τ_1 is found near 400 nm where the expected absorbance changes are the largest. The shape of the 65- μs (τ_2) component (Figure 7b) is very close to the spectrum predicted from the ferrocene-trapped semiquinone spectrum (Figure 2b). While the amplitude at τ_3 has a spectrum similar to τ_2 in the 398–435-nm range, its amplitude is close to zero at wavelengths longer than 450 nm (Figure 7b). The 398-nm peak in the τ_2 and τ_3 difference spectra do show the oxidation state change of UQ_A^- (Figure 7b). However, the lifetime correlated spectra shows that these kinetic components follow different shifts in the free-radical anion or protein spectra near 450 nm. The sum of the amplitudes at τ_2 and τ_3 qualitatively matches the spectrum predicted from the static Q_A^- and Q_B^- spectra (Figure 7d).

Temperature Dependence of Processes Associated with the Electron Transfer from Q_A^- to Q_B . The temperature dependence of the kinetic components was measured between 0 and 27 °C in both $MQ_A UQ_B$ and $UQ_A UQ_B$ RCs (Figure 8 and Table 1). The pH of the Tris buffer changes from pH 8 to 8.6 over the temperature range 22–5 °C. However, measurement of the rate as a function of pH shows that this should have negligible effect. In $MQ_A UQ_B$ RCs, the proportion of the electron transfer that occurs at τ_1 does not change with temperature (Figure 8b). The activation energy

of τ_1 is 3.8 ± 1.1 kcal/mol (Figure 8a) with a pre-exponential factor of $(2.2 \pm 0.3) \times 10^8 \text{ s}^{-1}$. The activation energy of τ_2 is 3.4 ± 0.6 kcal/mol with a pre-exponential factor of $(5.0 \pm 0.3) \times 10^6 \text{ s}^{-1}$ (Table 1). The activation energy of τ_3 is 7.1 ± 1.3 kcal/mol.

DISCUSSION

Biphasicity of $Q_A^- Q_B \rightarrow Q_A Q_B^-$ Electron Transfer

Electron Transfer from Q_A^- to Q_B When Q_A Is MQ . The analysis of the kinetic components of the spectral changes in the 398 to 480 nm region reveals three time scales for events connected to the electron transfer from MQ_A^- to UQ_B (Figure 9). Electron transfer in MQ_A RCs occurs in the two faster phases, with lifetimes of $3.5 \pm 0.9 \mu\text{s}$ (τ_1) and $80 \pm 15 \mu\text{s}$ (τ_2) at 22 °C. The lifetime correlated difference spectra in RCs (Figure 7a) look like the static MQ^- minus UQ^- spectrum in solution (Figure 3b) (31). This clearly identifies these components as individual phases of electron transfer.² The rate and pH dependence (not shown) of the 80- μs component is close to the traditionally assigned single lifetime for the electron transfer from UQ_A^- to UQ_B of 100–300 μs (7, 17, 30). However, the 3- μs phase is faster than what has been previously described in isolated UQ_A containing *Rb. sphaeroides* RCs (Figure 9), although similar rates and amplitudes for biphasic UQ_A^- to UQ_B electron transfer have been seen in chromatophores (45, 46). Similar fast rates have been reported for native *Rps. viridis* RCs, with electron transfer from MQ_A^- to UQ_B , occurring with lifetimes of 6 μs at pH 7 and 30 μs at pH 8 in membrane fragments (47) and 18 μs in whole cells (48) at pH 7. Possible mechanisms that can yield these distinct rates will be considered below.

Both τ_1 and τ_2 are also seen in the electrochromic response of the BPh, measured at 757 nm in MQ_A RCs. This

² M. S. Graige, G. Feher and M. Y. Okamura (Physics Department of University of California at La Jolla) determined the recovery of P's competence to initiate a second turnover of electron transfer in the presence of cytochrome c_2 in $MQ_A UQ_B$ reaction centers (RCs). This cannot occur until Q_A^- has been oxidized by Q_B (29, 30). Their results support the finding that a significant fraction of the reoxidation of Q_A^- occurs faster than 10 μs in these RCs.

wavelength is near the isobestic point for the $P^+Q_A^-$ spectrum, and as discussed previously (26, 45, 46), it monitors the electrostatic perturbation of the BPh optical absorption associated with the formation of the Q_B^- state. Charge-compensating events will attenuate this signal, and differences between the electron-transfer and charge-compensating events will add kinetic complexity. However, the close correspondence between the lifetimes determined in the near-UV and at 757 nm supports the interpretation that changes at this near-IR wavelength primarily detect electron transfer. The relative amplitudes of the kinetic components in the near-UV and at 757-nm need not be the same, since the near UV and 757 nm signals need not have the same dependence on dielectric and protonation state changes in the cofactor surroundings.

There is a third kinetic component present near 398 nm, $\tau_3 = 200\text{--}600 \mu\text{s}$ (22°C), which also depends on the presence of a functional Q_B . The spectrum of the absorbance changes associated with τ_3 shows clearly that this is not electron transfer (Figure 7a). Thus, electron transfer and slower protein responses are kinetically well-separated in MQ_A containing RCs. A kinetic separation is also seen in the near-IR transient spectra. Measurements at 770 nm (data not shown) with lifetimes at 6°C of approximately $60 \mu\text{s}$ and 2 ms show a distinct lag compared to those at 757 nm where the lifetimes are 6.6, 205, and $950 \mu\text{s}$. Previous measurements in chromatophores have shown that the 770-nm transients reflect quenching of the electrochromism associated with the Q_B^- state, while transients at 757 nm monitor both electron transfer and charge-compensating events (45, 46). Hence, measurements in the near-UV and near-IR both support the conclusion that the changes at τ_1 are mostly due to electron transfer, and electron transfer and charge compensation are mixed in τ_2 , while little or no electron transfer occurs at τ_3 in MQ_AUQ_B RCs.

Electron Transfer from Q_A^- to Q_B When Q_A Is UQ. Measurement and assignment of Q_A^- to Q_B electron transfer and accompanying nonelectron-transfer events is significantly more difficult with RCs containing UQ_AUQ_B than those containing MQ_AUQ_B . Rather than a change in the primary optical signal the UQ_A^- absorbance is simply red-shifted 3 nm relative to UQ_B^- . UQ_A^- is also associated with an absorption peak near 398 nm, which is an isobestic point of the P^+-P signal. The origin of this peak is unknown, but it appears not to be a property of the UQ^- itself, and hence apparently arises from an electrochromic response of another RC cofactor to the oxidation state of Q_A . In addition, the assignment of changes at 398 nm to processes occurring after electron transfer must be considered in UQ_AUQ_B RCs since this wavelength is seen to report nonelectron-transfer events in the MQ_AUQ_B RCs.

Optical transients in RCs with UQ_AUQ_B show kinetic components comparable to τ_2 and τ_3 in MQ_AUQ_B RCs (Figure 7b). In contrast to the results in MQ_AUQ_B RCs, there is less distinction between the spectra of τ_2 and τ_3 (Figure 7). The coincidence of the kinetics of electron-transfer and charge-compensating events in UQ_AUQ_B RCs is also supported by measurements in the near-IR. These show equivalent, complex kinetics occurring on the time scales of τ_2 and τ_3 throughout the near-IR region, including measurements at 757 nm monitoring both electron transfer and charge compensation, and at 770 nm which responds

selectively to charge compensation events (45, 46). A small fraction of the changes at 398 and 757 nm may occur faster than what can be measured ($<1 \mu\text{s}$). However, any burst phase accounts for at most 15% of the signal.

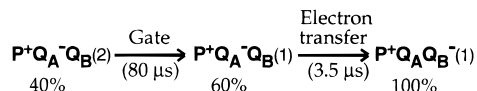
Nonelectron-Transfer Events Occurring at τ_2 and τ_3 . It is not possible to assign the source of the nonelectron-transfer components from the near-IR or near-UV spectra. However, previous studies have identified processes such as proton transfer and protein relaxation occurring with lifetimes similar to τ_3 which may underlie the spectral changes observed here. Thus, Hienerwadel et al. (20, 21) have made time-resolved IR measurements in native *Rb. sphaeroides* RCs (4°C , pH 7–7.5) under conditions where τ_2 here is $120 \pm 15 \mu\text{s}$ and τ_3 is $\approx 1 \text{ ms}$ (Figure 9b). Several peaks between 1780- and 1430-cm⁻¹ change with lifetimes of $\approx 170 \mu\text{s}$ ($\tau_{1/2} = 120 \mu\text{s}$). The carboxylic acid group of Glu L212 (1725 cm⁻¹) was protonated in $260 \mu\text{s}$ (25%) and 1.4 ms (75%) (21). The 170–260- μs component, comparable to τ_2 here, was assigned to events that occur with the electron transfer itself and the slow component (τ_3 here) represents later proton transfers or conformational changes. In addition, pH indicator dye shows H^+ uptake at $10^4\text{--}10^5 \text{ s}^{-1}$ following $P^+Q_A^-$ formation (49). Other methods also show transients on the time scale of τ_3 that appear to be protein relaxation following electron transfer. The electrochromic shift of the BPh absorbance that monitors Q_B^- formation is diminished at $100\text{--}300 \mu\text{s}$ ($\approx 20^\circ\text{C}$). This is indicative of protein relaxation screening BPh_M from Q_B^- (45). Brzezinski et al. observed a voltage change with $\tau \approx 200 \mu\text{s}$ (at 20°C) following the formation of $P^+Q_A^-$ or $P^+Q_B^-$ (50). This component diminished the total voltage change for the formation of $P^+Q_A^-$ (a 23 Å distance) by about 10%.

Activation Energy of the Events Associated with Electron Transfer from Q_A^- to Q_B . Both phases of the electron-transfer reaction have relatively small activation energies of 3–4 kcal/mol while E_a is significantly larger for τ_3 (Table 1). There are few earlier-published values for the activation energy of the electron transfer from Q_A^- to Q_B . Mancino et al. (42) measured a value of 14.3 kcal/mol ($\tau_{AB} = 200 \mu\text{s}$ at 750 nm), significantly larger than the E_a for τ_2 . Their measurements were modeled by a single exponential, mixing τ_2 and τ_3 . A single-component fit of the data reported here from 0–2 ms yields a value of 8.1 kcal/mol. Recent measurements at 757 nm in UQ_A RCs are in better agreement with the results reported here, with an $E_a = 4.5 \text{ kcal/Mol}$ ($\tau = 25\text{--}40 \mu\text{s}$ at 20°C) and $E_a = 11 \text{ kcal/Mol}$ ($\tau = 210\text{--}240 \mu\text{s}$ at 20°C) (26), identified with τ_2 and τ_3 , respectively.

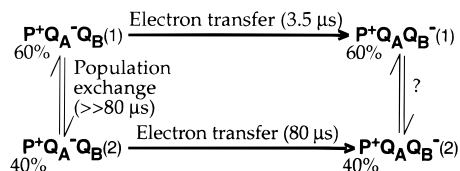
Kinetic Models That Yield Two Rates for Electron Transfer from Q_A^- to Q_B

The electron transfer in MQ_A RCs has two distinct, temporally well-separated, kinetic components: $3.5 \pm 0.9 \mu\text{s}$ (60%) and $80 \pm 15 \mu\text{s}$ (40%). Two different kinetic schemes can account for the observed rates, each of which requires two populations of RCs. In a series or gated mechanism (Scheme 1), the 80- μs phase represents transformation from an inactive (RC_2) to an active (RC_1) state which then undergoes electron transfer in 3 μs . Initially, 60% of the RCs are in the active state. In a parallel mechanism (Scheme 2), both populations undergo electron transfer at 3 μs (RC_1) and 80 μs (RC_2), respectively. The

Scheme 1



Scheme 2



equilibration of the two forms of RCs would occur on a time scale much longer than $80\ \mu s$. While the data appears to favor a gated mechanism, we cannot yet rule out the parallel scheme.

Data Supporting the Gated Mechanism. Here electron transfer occurs in $3\ \mu s$, while changes in the inactive fraction of protein required for electron transfer determine the τ_2 lifetime. As described above, while spectral changes in the near-UV show electron transfer occurs at both τ_1 and τ_2 , there are no changes at τ_1 at 770 nm, a wavelength which only monitors protein relaxation but does not respond directly to electron transfer. However, changes at 770 nm do occur at τ_2 . Thus, changes such as proton distribution or protein conformation occur in the second phase of electron transfer. In the gated model, these changes are required and determine the rate for electron transfer in RC_2 RCs.

Data Opposing the Parallel Mechanism. Charge recombination from the $P^+Q_AQ_B^-$ state (k_{BP}) can measure K_{AB} , the equilibrium constant between $Q_A^-Q_B$ and $Q_AQ_B^-$ (eqn 1). k_{BP} in the MQ_AUQ_B RCs is close to a single exponential, so there is little difference between K_{AB} in the populations of RCs that react at τ_1 and τ_2 . The most straightforward explanation is that there is only one $P^+Q_AQ_B^-$ state, supporting the gated mechanism. The parallel mechanism requires either similar K_{AB} 's in RC_1 and RC_2 or a conformation change after the formation of Q_B^- but before charge recombination ($<1\ s$) yielding one $P^+Q_AQ_B^-$ state. The 60:40 population of RC_2 and RC_1 would need to be restored during the 2 min between flashes.

Data Opposing the Gated Mechanism. Much of the data supports a mechanism where the electron transfer occurs from one population of RCs. However, two pieces of data are difficult to accommodate in this mechanism. The E_a for the $80\text{-}\mu s$ component is only $3.4\ \text{kcal/mol}$, the same as for the $3\text{-}\mu s$ phase. Thus, whatever changes occur at τ_2 to transform RC_2 to RC_1 must be accomplished with only a small activation energy, although there may still be a substantial entropy of activation. Also, the relative amplitude of the two phases does not change with temperature (Figure 8). This requires a negligible enthalpy difference between RC_1 and RC_2 to maintain the temperature-independent equilibrium constant.

Variation in the Kinetic Parameters That Distinguish RC_1 and RC_2 . If electron transfer is rate-limiting for τ_1 , then electron-transfer theory can provide a rough estimate of the differences between RC_1 and RC_2 that could yield a 20-fold slower τ_2 . In the simplest formulation of the theory by Marcus $k_{AB} = Ce^{-\beta R} \exp(-(\Delta G - \lambda)^2/4k_B T)$, where $C \approx 10^{13}/s$, ΔG the free-energy difference between reactants and prod-

ucts, λ the reorganization energy, R the distance between the electron donor (Q_A) and acceptor (Q_B), β the fall-off of the rate with distance, T the temperature, and k_B Boltzman's constant (51–54). For this reaction, the $-\Delta G$ of $60\text{--}90\ \text{meV}$ is much less than λ , which is estimated to be $700\text{--}1300\ \text{eV}$ (53, 55). The rate will increase as $-\Delta G$ approaches λ . A reduction in λ of $\approx 300\ \text{meV}$ or increase in exothermicity of $\approx 200\ \text{meV}$ could increase the rate by 20-fold. Alternatively, if β is $1.4\ \text{\AA}^{-1}$ (53), a $2.7\text{-}\text{\AA}$ change in distance from Q_A to Q_B could account for the difference in rates extrapolated to $-\Delta G = \lambda$ of $2.2 \times 10^8\ \text{s}^{-1}$ (for τ_1) and $5.0 \times 10^6\ \text{s}^{-1}$ (for τ_2) (see Results Section). The rates extrapolated to infinite temperature provide the estimates of the rates at $-\Delta G = \lambda$ (Figure 8).

What Might Yield RCs with Different Electron-Transfer Rates

Electron transfer from Q_A^- to Q_B occurs at more than a single rate in all RCs. The rates vary by at least 20-fold. If electron transfer is mixed into the processes occurring at τ_3 , the rate would vary by more than 100-fold. We do not yet know what causes RCs to switch from one rate to another. However, a number of perturbations have been found to change the distribution of rates. In UQ_AUQ_B RCs, the electron-transfer rate changes from faster and clearly biexponential in chromatophores to slower, more nearly single exponential in purified UQ_A RCs (26, 45, 46). At room temperature, electron transfer and relaxation events are mixed in this single phase. Since relaxation processes have a larger activation energy on cooling, electron transfer becomes more clearly separated from other events (Figure 6) (26, 45). Dehydration of isolated UQ_A RCs by increasing the solution osmotic strength shifts the electron transfer toward the more native faster τ_1 and τ_2 lifetimes (26). These are global changes to the protein surroundings and so do not point to a specific molecular switch between the RC forms where electron transfer is at τ_1 and τ_2 or those where it is at τ_2 and τ_3 . For reasons that are not yet understood, reconstitution of MQ into the Q_A site in isolated RCs yields electron-transfer kinetics that appear to be closer to the *in vivo* reaction than that found in isolated UQ_A RCs. The similarity of the kinetics could be fortuitous, or it could be a reflection of the preference of the site for MQ . MQ binds more tightly than UQ to the Q_A site in isolated RCs (37) and is preferred at this site in bacteria such as *Rps. viridis*, which synthesize both quinones (33). Alternately, reconstitution with the larger MQ_A may remove bound water, producing effects similar to that seen in isolated RCs at high osmolarity where τ_1 is seen (26). The ability to switch the proportion of fast- and slow-reacting RCs by quinone replacement will provide an opportunity to characterize the changes in the RCs that yield the different rates in future experiments.

Differences between RCs with MQ_A and UQ_A . The distinctly different patterns of transient near-UV and near-IR spectra for UQ_AUQ_B RCs and MQ_AUQ_B RCs suggest that these RCs differ in the rate-determining steps for electron transfer from Q_A^- to Q_B . In isolated UQ_AUQ_B RCs at room-temperature, both electron- and nonelectron-transfer events are distributed over the τ_2 and τ_3 lifetimes, while in MQ_AUQ_B RCs electron transfer occurs at τ_1 and τ_2 , while nonelectron-transfer events occur at τ_2 and τ_3 . This difference is

unexpected. Many previous experiments have shown that MQ_A RCs behave similarly to UQ_A RCs. Structural comparisons show (1) similar interactions between Q_A and the protein in the crystal structures of *Rps. viridis* RCs where MQ is the native Q_A and in *Rb. sphaeroides* RCs with UQ_A (35), (2) the same hydrogen bonding pattern and cofactor orientation in *Rb. sphaeroides* RCs with native UQ_A or reconstituted MQ_A (personal communication, Guenter Fritzsch), and (3) similar protein changes for both UQ_A and MQ_A in Q_A^- minus Q_A FTIR difference spectra in *Rb. sphaeroides* RCs (56). In addition, functional studies show (1) the free energy for electron transfer from MQ_A^- to UQ_B is only 30 meV more favorable than that with UQ_A , (2) the quantum yield for electron transfer from BPh^- to MQ_A is 100% even at cryogenic temperature where the quinone must be rigidly held in the binding site (57), and (3) electron transfer from MQ_A^- to P^+ is as well-characterized by a single exponential as in native RCs even at cryogenic temperatures (58). FTIR measurements of the hydrogen bonding of MQ_A and UQ_A show the clearest differences between the quinones. One of the UQ carbonyls shifts by $>30\text{ cm}^{-1}$ and the other by $<5\text{ cm}^{-1}$ when it is bound to the Q_A site. Thus, UQ_A^- appears to make only one, strong hydrogen bond, probably with the proximal carbonyl (O_4) (59, 60). In contrast, MQ_A^- carbonyls each shift by $\approx 10-20\text{ cm}^{-1}$, so it appears to make two hydrogen bonds (56). This raises the possibility that the second hydrogen bond could fix Q_A firmly in the correct position for rapid electron transfer.

Possible Sources of Heterogeneity in the Q_A Pocket. Measurements of the electron transfer between P and Q_A suggest there is only small functional heterogeneity for Q_A (61–64). Extensive analysis of the charge recombination to the ground state in $P^+Q_A^-$ RCs at room temperature shows that the kinetics for this reaction can be fit with two rates that vary by at most a factor of 3 (62, 65, 66). The free energy of the Q_A^- state can be estimated from the rate of the charge recombination in $P^+Q_A^-$ RCs reaction when Q_A is replaced with quinones ≈ 150 meV lower in potential than UQ_A (34, 65–69). Heterogeneity in the Q_A^- free energy of ≈ 20 meV in *Rb. sphaeroides* (65) and ≈ 30 meV in *Rps. viridis* RCs (66, 70) has been found. It seems unlikely that this small difference in reaction free energy is sufficient to account for the 20-fold difference between τ_1 and τ_2 .

Differences in hydrogen bonding of the quinones could change the electron-transfer rates. Only one of the two Q_A carbonyls is needed for function (57, 58, 71, 72). A Q_A^- with stronger hydrogen bonds will be more rigidly held in the site, which may reduce λ , facilitating faster electron transfer. His M219, the proximal hydrogen bond donor, is a ligand of the non-heme iron connecting the Q_A and Q_B sites (35, 54, 73). Differences in this bridge for electron transfer, in RC_1 and RC_2 , could modify the rate by changing $e^{-\beta R}$ (53, 54).

Possible Sources of Heterogeneity in the Q_B Pocket. Two electron-transfer rates, each with $\approx 50\%$ of the total amplitude, could result from two Q_B binding sites with similar quinone affinities. In the parallel mechanism, both sites would be active; in the gated mechanism, movement from inactive to active site occurs at τ_2 . Several distinct binding sites have been shown. FTIR measurements in *Rb. sphaeroides* RCs suggest 25% of Q_B 's have weak interactions between the protein and quinone carbonyls, while 75% have

strong interactions (74). X-ray crystal structures of *Rps. viridis* RCs show two sites for the competitive inhibitor *o*-phenanthroline, and seven sites for ubiquinone-1 (75) (for review see ref 35). For *Rb. sphaeroides* RCs, Allen et al. (76) and El-Kabbani et al. (77) located Q_B at a position close to where it is found in *Rps. viridis* RCs (35) in an inner binding site. In contrast, Ermler et al. (78) and Stowell et al. (79, 80) have found $Q_B \approx 3.5\text{ \AA}$ further away from Q_A in the hydrophobic entrance of the Q_B binding pocket. The quinone is in the inner site in light-activated RCs and the outer site in dark-adapted protein (80).

In the gated mechanism, the quinone must move between the binding sites that distinguish RC_1 from RC_2 in $80\text{ }\mu\text{s}$ with an E_a of only 3.5 kcal/mol. There are negligible differences in the protein in structures with and without Q_B (35) or with the quinone in different locations (80). This is consistent with a low barrier for quinone relocation. However, the position of the tail in the "light" and "dark" adapted structures shows the quinone flipped by 180° along an axis between the quinone C_2 and C_3 (35, 80). In the inner site, O_4 is hydrogen bonded to His L190, while O_1 is closer to the His in the outer site. For this rearrangement to convert RC_2 into RC_1 , it needs to occur in $80\text{ }\mu\text{s}$ with a 3–4 kcal enthalpy of activation. The large difference between the quinone orientations in the light and dark structures may make this difficult. In the parallel mechanism, both binding sites would be active. However, K_{AB} must be similar at each active sites to maintain a single rate for charge recombination from $P^+Q_B^-$ (k_{BP}). This seems unlikely since there are two possible hydrogen bonds to Q_B in the inner site and one in the outer site (78–80). The electron transfer could occur to both locations, with the semiquinone moving to occupy one site. This also requires release of Q_B^- from the pocket so that it can flip over.

Possible Sources of Heterogeneity in the Protein. The complexity of the electron-transfer kinetics from Q_A^- to Q_B may reflect heterogeneity of the electrostatic environment of Q_B . This region of the protein is characterized by an interconnected group of acidic residues including Glu L212, Asp L213, and Glu H173 (15, 16, 22). Calculations of the proton occupancy of these residues show several protonation states with similar energies, indicating RCs may exist in a variety of substates. Glu L212 is the nearest acid in the cluster to Q_B and its ionization is predicted to destabilize Q_B^- , disallowing electron transfer (15, 22). Calculations predicted a role for this acid in the formation of Q_B^- (22), subsequently confirmed by FTIR and time-resolved IR measurements showing the acid undergoing substoichiometric protonation (0.3–0.6 H^+/RC) at $\approx \tau_2$ (21, 23). These measurements could support a role for Glu L212 in a gated mechanism where protonation of this site controls the rate of the electron transfer at τ_2 . The remaining fraction, if it is protonated in the ground state, could react at τ_1 (15, 16). In addition, τ_2 depends on pH, slowing above pH 9. Thus, proton uptake is important in this phase of electron transfer (7, 27, 30, 81). In contrast, no significant pH dependence at τ_1 is observed from pH 6–11 (data not shown). Interestingly, the fast, microsecond electron transfer from MQ_A to UQ_B in native *Rps. viridis* RCs also shows only a weak pH dependence (48, 82).

ACKNOWLEDGMENT

We thank Bob Alfano for the timely, and much appreciated gift of a $50\ \Omega$ resistor, Dewey Holten for many helpful discussions and ready equipment loans, Mark Paddock, Mike Graige, Mel Okamura, and Colin Wraight for stimulating discussions.

REFERENCES

- Feher, G., Allen, J. P., Okamura, M. Y., and Rees, D. C. (1989) *Nature* **339**, 111–116.
- Gunner, M. R. (1991) *Curr. Top. Bioenerg.* **16**, 319–367.
- Blankenship, R. E., Madigan, M. T., and Bauer, C. E. (1995) *Anoxygenic Photosynthetic Bacteria*, Vol. 2, Kluwer Academic Publishers, Dordrecht.
- Maroti, P., and Wraight, C. A. (1988) *Biochim. Biophys. Acta* **934**, 314–328.
- McPherson, P. H., Okamura, M. Y., and Feher, G. (1988) *Biochim. Biophys. Acta* **934**, 348–368.
- Graige, M. S., Paddock, M. L., Bruce, J. M., Feher, G., and Okamura, M. Y. (1996) *J. Am. Chem. Soc.* **118**, 9005–9016.
- Wraight, C. A. (1979) *Biochim. Biophys. Acta* **548**, 309–327.
- Wraight, C. A. (1977) *Biochim. Biophys. Acta* **495**, 525–531.
- Kleinfeld, D., Okamura, M. Y., and Feher, G. (1985) *Biochim. Biophys. Acta* **809**, 291–310.
- Okamura, M. Y., and Feher, G. (1995) in *Anoxygenic Photosynthetic Bacteria* (Blankenship, R. E., Madigan, M. T., and Bauer, C. E., Eds.) pp 231–257, Kluwer Academic Publishers: Dordrecht.
- Cramer, W. A., and Knaff, D. B. (1991) *Energy Transduction in Biological Membranes: A Textbook of Bioenergetics*, Springer-Verlag: New York.
- Nicholls, D. G., and Ferguson, J. S. (1992) *Bioenergetics 2*, Academic Press Limited, London.
- Takahashi, E., and Wraight, C. A. (1994) *Adv. Mol. Cell Biol.* **10**, 197–251.
- Breton, J., and Vermélio, A. (1988) *The Photosynthetic Bacterial Reaction Center: Structure and Dynamics*, Plenum Press, New York.
- Beroza, P., Fredkin, D. R., Okamura, M. Y., and Feher, G. (1995) *Biophys. J.* **68**, 2233–2250.
- Lancaster, C. R. D., Michel, H., Honig, B., and Gunner, M. R. (1996) *Biophys. J.* **70**, 2469–2492.
- Vermélio, A., and Clayton, R. K. (1977) *Biochim. Biophys. Acta* **461**, 159–165.
- Hales, B. J., and Case, E. E. (1981) *Biochim. Biophys. Acta* **637**, 291–302.
- Lubitz, W., Abresch, E. C., Debus, R. J., Isaacson, R. A., Okamura, M. Y., and Feher, G. (1985) *Biochim. Biophys. Acta* **808**, 464–469.
- Hienerwadel, R., Thibodeau, D., Lenz, F., Nabedryk, E., Breton, J., Kreutz, W., and Mantele, W. (1992) *Biochemistry* **31**, 5799–5808.
- Hienerwadel, R., Grzybek, S., Fogel, C., Kreutz, W., Okamura, M. Y., Paddock, M. L., and Breton, J. (1995) *Biochemistry* **34**, 2832–2843.
- Gunner, M. R., and Honig, B. (1992) in *The Photosynthetic Bacterial Reaction Center: Structure, Spectroscopy and Dynamics II* (Breton, J., and Vermeglio, A., Eds.) pp 403–410, Plenum Press, New York.
- Nabedryk, E., Breton, J., Hienderwadel, R., Fogel, C., Mantele, W., Paddock, M. L., and Okamura, M. Y. (1995) *Biochemistry* **34**, 14722–14732.
- Okamura, M. Y., and Feher, G. (1992) *Annu. Rev. Biochem.* **61**, 861–896.
- Bensasson, R., and Land, E. J. (1973) *Biochim. Biophys. Acta* **325**, 176–181.
- Tiede, D. M., Vazquez, J., Cordova, J., and Marone, P. A. (1996) *Biochemistry* **35**, 10763–10775.
- Takahashi, E., Maroti, P., and Wraight, C. A. (1992) in *Electron and Proton Transfer in Chemistry and Biology* (Muller, A., Ed.) pp 219–236, Elsevier, New York.
- Tiede, D. M., and Hanson, D. K. (1992) in *The Photosynthetic Reaction Center II* (Breton, J., and Vermeglio, A., Eds.) pp 341–350, Plenum Press, New York.
- Parson, W. W. (1969) *Biochim. Biophys. Acta* **189**, 384–396.
- Kleinfeld, D., Okamura, M. Y., and Feher, G. (1984) *Biochim. Biophys. Acta* **766**, 126–140.
- Patel, K. B., and Willson, R. L. (1973) *J. Chem. Soc.* **69**, 814–825.
- Swallow, A. J. (1982) in *Function of Quinones in Energy Conserving Systems* (Trumppower, B. L., Ed.) pp 59–72, Academic Press, New York.
- Shopes, R. J., and Wraight, C. A. (1985) *Biochim. Biophys. Acta* **806**, 348–356.
- Woodbury, N. W., Parson, W. W., Gunner, M. R., Prince, R. C., and Dutton, P. L. (1986) *Biochim. Biophys. Acta* **851**, 6–22.
- Lancaster, C. R. D., Ermler, U., and Michel, H. (1995) in *Anoxygenic Photosynthetic Bacteria* (Blankenship, R. E., Madigan, M. T., and Bauer, C. E., Eds.) pp 503–526, Kluwer Academic Publishers, Dordrecht.
- Breton, J., and Nabedryk, E. (1996) *Biochim. Biophys. Acta* **1275**, 84–90.
- Warncke, K., Gunner, M. R., Braun, B. S., Gu, L., Yu, C., Bruce, J. M., and Dutton, P. L. (1994) *Biochemistry* **33**, 7830–7841.
- Giangiacomo, K. M., and Dutton, P. L. (1989) *Proc. Natl. Acad. Sci. U.S.A.* **86**, 2658–2662.
- Clayton, R. K., and Wang, R. T. (1971) *Methods Enzymol.* **23**, 696–704.
- Okamura, M. Y., Isaacson, R. A., and Feher, G. (1975) *Proc. Natl. Acad. Sci. U.S.A.* **72**, 3492–3496.
- McComb, J. C., Stein, R. R., and Wraight, C. A. (1990) *Biochim. Biophys. Acta* **1015**, 156–171.
- Mancino, L. J., Dean, D. P., and Blankenship, R. E. (1984) *Biochim. Biophys. Acta* **764**, 46–54.
- Slooten, L. (1972) *Biochim. Biophys. Acta* **275**, 208–218.
- Clayton, R. K., and Straley, S. C. (1972) *Biophys. J.* **12**, 1221–1234.
- Tiede, D. M., Gallo, D. M., and Hanson, D. K. (1997) *Biophys. J.* **72**, A248.
- Tiede, D. M., Utschig, L., Hanson, D. K., and Gallo, D. M. (1997) submitted to *Photosynth. Res.*
- Carithers, R. P., and Parson, W. W. (1975) *Biochim. Biophys. Acta* **387**, 194–211.
- Leibl, W., Sinning, I., Ewald, G., Michel, H., and Breton, J. (1993) *Biochemistry* **32**, 1958–1964.
- Maroti, P., and Wraight, C. A. (1997) *Biophys. J.* **73**, 367–381.
- Brzezinski, P., Okamura, M. Y., and Feher, G. (1992) in *The Photosynthetic Bacterial Research Center II* (Breton, J., and Vermeglio, A., Eds.) pp 321–330, Plenum Press, New York.
- Devault, D. (1980) *Q. Rev. Biophys.* **13**, 387–564.
- Marcus, R. A., and Sutin, N. (1985) *Biochim. Biophys. Acta* **811**, 265–322.
- Moser, C. C., Keske, J. M., Warncke, K., Farid, R., and Dutton, P. L. (1992) *Nature* **355**, 796–802.
- Onuchic, J. N., Beratan, D. N., Winkler, J. R., and Gray, H. B. (1992) *Ann. Rev. Biophys. Biomol. Struct.* **21**, 349–377.
- Labahn, A., Paddock, M. L., McPherson, P. H., Okamura, M. Y., and Feher, G. (1994) *J. Phys. Chem.* **98**, 3417–3423.
- Breton, J., Burie, J., Berthomieu, C., Berger, G., and Nabedryk, E. (1994) *Biochemistry* **33**, 4953–4965.
- Gunner, M. R., and Dutton, P. L. (1989) *J. Am. Chem. Soc.* **111**, 3400–3412.
- Gunner, M. R., Robertson, D. E., and Dutton, P. L. (1986) *J. Phys. Chem.* **90**, 3783–3795.
- Brudler, R., de Groot, J. M., van Liemt, W. B. S., Steggerda, W. F., Esmeijer, R., Gast, P., Hoff, A. J., Lugtenburg, J., and Gerwert, K. (1994) *EMBO J.* **13**, 5523–5530.
- Breton, J., Claude, B., Burie, J., Nabedryk, E., and Mioskowski, C. (1994) *Biochemistry* **33**, 14378–14386.
- Morrison, L. E., and Loach, P. A. (1978) *Photochem. Photobiol.* **27**, 751–757.

62. Parot, P., Thiery, J., and Vermèglio, A. (1987) *Biochim. Biophys. Acta* 893, 534–543.
63. Gao, J., Shopes, R. J., and Wright, C. A. (1991) *Biochim. Biophys. Acta* 1056, 259–272.
64. Baciou, L., and Sebban, P. (1995) *Photochem. Photobiol.* 62, 271–278.
65. Sebban, P. (1988) *Biochim. Biophys. Acta* 936, 124–132.
66. Sebban, P., and Wright, C. A. (1989) *Biochim. Biophys. Acta* 974, 54–65.
67. Gunner, M. R., Tiede, D. M., Prince, R. C., and Dutton, P. L. (1982) in *Function of Quinones in Energy Conserving Systems* (Trumper, B. L., Ed.) pp 265–269, Academic Press, New York.
68. Kleinfeld, D., Okamura, M. Y., and Feher, G. (1985) *Biophys. J.* 48, 849–852.
69. Franzen, S., Goldstein, R. F., and Boxer, S. G. (1990) *J. Phys. Chem.* 94, 5135–5149.
70. Shopes, R. J., and Wright, C. A. (1987) *Biochim. Biophys. Acta* 893, 409–425.
71. Gunner, M. R., Braun, B. S., Bruce, J. M., and Dutton, P. L. (1985) in *Antennas and Reaction Centers of Photosynthetic Bacteria* (Michel-Beyerle, M. E., Ed.) pp 298–305, Springer-Verlag, Berlin.
72. Warncke, K., and Dutton, P. L. (1993) *Biochemistry* 32, 4769–4779.
73. Moser, C. C., Page, C. C., Chen, X., and Dutton, P. L. (1997) *J. Biol. Inorg. Chem.*, in press.
74. Brudler, R., de Groot, H. J. M., van Liemt, W. B. S., Hoff, A. J., Lugtenburg, J. L., and Gerwert, K. (1995) *FEBS Lett.* 370, 88–92.
75. Deisenhofer, J., Epp, O., Miki, R., and Michel, H. (1985) *Nature* 318, 618–624.
76. Allen, J. P., Feher, G., Yeates, T. O., Komiya, H., and Rees, D. C. (1988) *Proc. Natl. Acad. Sci. U.S.A.* 85, 8487–8491.
77. El-Kabbani, O., Chang, C.-H., Tiede, D., Norris, J., and Schiffer, M. (1990) *Biochemistry* 30, 5361–5369.
78. Ermler, U., Fritzsch, G., Buchanan, S. K., and Michel, H. (1994) *Structure* 2, 925–936.
79. Abresch, E. C., Stowell, M. H. B., McPhillips, T. M., Rees, D. C., Soltis, S. M., and Feher, G. (1997) *Biophys. J.* 72, A8.
80. Stowell, M. H. B., McPhillips, T. M., Rees, D. C., Soltis, S. M., Abresch, E. C., and Feher, G. (1997) *Science* 276, 812–816.
81. Paddock, M. L., Rongey, S. H., Feher, G., and Okamura, M. Y. (1989) *Proc. Natl. Acad. Sci. U.S.A.* 86, 6602–6606.
82. Mathis, P., Sinnig, I., and Michel, H. (1992) *Biochim. Biophys. Acta* 1098, 151–158.

BI971699X